Structure and symmetry in coherent perfect polarization rotation

Michael Crescimanno,* Chuanhong Zhou, James H. Andrews, and Michael A. Baker
Department of Physics and Astronomy, Youngstown State University, Youngstown, Ohio 44555-2001, USA
(Received 11 September 2014; published 29 January 2015)

Theoretical investigations of different routes to coherent perfect polarization rotation illustrate its phenomenological connection with coherent perfect absorption. Our study of systems with broken parity, layering, combined Faraday rotation and optical activity, or a rotator-loaded optical cavity highlights their similarity and suggests alternate approaches to improving and miniaturizing optical devices.

DOI: 10.1103/PhysRevA.91.013845 PACS number(s): 42.25.Bs, 78.20.Ls, 42.25.Hz, 78.67.Pt

I. INTRODUCTION

Coherent perfect polarization rotation (CPR) [1] is a conservative, reversible example of a multiport, maximally efficient, optical mode conversion process. As such, it shares phenomenological correspondences with the coherent perfect absorber (CPA, also called the antilaser) [2,3], which has been well studied [4–7]. While many optical devices such as laser wavelength locks, field sensors, optical isolators, and modulators are based on the nonreciprocal nature of Faraday rotation, one way to improve all of these devices is to process all of the incident light coherently. CPR-based design is an intrinsically multi (input)–port approach that combines the nonreciprocal nature of the Faraday effect with interference to convert *all* of the incident light into its orthogonal polarization. An example of the basic two-port CPR device is shown in Fig. 1.

For the apparatus shown in Fig. 1, one still must tune the magnetic field to specific values to achieve complete conversion of the polarization. The required field is significantly below that of a single port rotator, however. For one example, the complete conversion of one polarization into its orthogonal polarization using an uncoated terbium gallium garnet slab requires only 60% of the field-length product needed for the same rotation in just the transmitted light [1]. Achieving complete polarization conversion at a lower field-length product is technologically useful because it is precisely the seeming "incompressibility" of this product and the modest Verdet coefficients of commercially available optical materials that pose a major obstacle to the diffusion of single-port designs into integrated optical assemblies and low-cost devices. The primary motivation for the work reported here is to quantify in typical one-dimensional optical geometries how CPR-based optical design significantly lowers the field-length product. We characterize the reduction of the threshold field-length product at which coherent perfect processes first occur consequent to specific design choices in optical dispersion, structural dispersion, broken parity, and localization.

A second motivation for this study is to reveal general principles common among coherent perfect processes. Enlarging the context for these phenomena builds intuition useful for finding routes to improving optical devices. We do this primarily by comparing and contrasting CPR and CPA. Note that in both CPR and CPA, a tunable time-odd optical process (magneto-optical rotation for CPR versus absorption in CPA) is combined with multiport wave interference to achieve perfectly efficient mode conversion (to orthogonal polarization in CPR and to electronic excitation in CPA). Among other commonalities between CPA and CPR are their critical dependence on the relative optical phases among the input light fields. As in the single-port case of critical coupling, CPA and CPR both require a particular (hereafter "threshold") magnitude for the time-odd process. In both CPR and CPA the conversion efficiency has a resonance-like structure. Also, for a fixed wavelength going both above or below the threshold makes complete conversion impossible. Because this "resonance" is not associated with a particular decay time scale, coherent perfect resonances are intrinsically zero width. Many of the remaining phenomenological differences between CPR and CPA can be traced to the fact that CPR is Hermitian, whereas CPA is not. For example, the time reverse of CPA is lasing, whereas the time reverse of CPR is CPR itself.

The understanding of CPA phenomena in diverse optical systems has advanced steadily. Theory relates CPA states to self-dual spectral singularities [2,8] of the S matrix. The CPA threshold's dependence on the depth of the sample is well understood theoretically, and this dependence has been modeled in complex (but still linear) media, such as gold-silica composites and other plasmonic systems [9,10], and nonlinear media [11]. Both ordinary and $\mathcal{PT}$-symmetric systems elicit a diverse set of CPA phenomena, with those most relevant to CPA thresholds including gratings [12–15], surface plasmonic polaritons [16], photonic crystals [17], near-zero-ϵ materials [18], cavities with absorbers [19], controlled disorder or other spatial ordering [20,21], and very thin absorptive layers [22]. Some of these ideas are also being explored for technological uses including all optical switching [23–27] and CPA enhancement of photoluminescence [28].

After fixing notation and giving a brief review of the basic phenomena, Sec. III explores CPR and contrasts it with CPA in different optical environments, highlighting the roles played by dispersion, parity, and transport of mixed symmetry type. In Sec. III A we focus on coherent perfect phenomena in model multilayer systems, followed, in Sec. III B, by breaking parity in two different ways (first, softly with randomness and, then, explicitly with trinary multilayers). Thematically up to that point, one sees a direct correspondence between the layering effects on CPR and CPA states and thresholds. Subtle differences between the two are discussed in one archetypal example combining CPR and optical rotation in Sec. III C.

*dcphtn@gmail.com

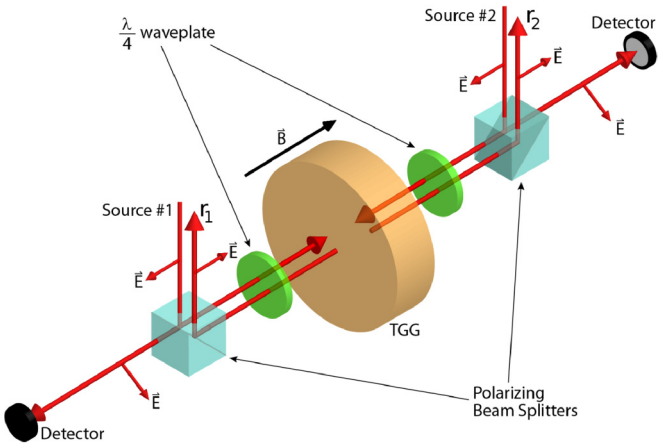

FIG. 1. (Color online) Basic schematic of a two-port CPR device. Not shown are attenuators and delay plates that balance the input field's amplitude and phase. When the CPR resonance condition is achieved, the reflected light r_1 and r_2 vanishes.

A brief conclusion highlights new directions that may be prompted by this study.

II. NOTATION AND PRELIMINARIES

We use matrices to represent linear transport and work in the basis where the local field (complex) amplitudes for light traveling along the $\hat{z}$ axis are $\vec{v} = (E_x, H_y, E_y, -H_x)$. In terms of the individual polarization and motional states, we use $\vec{e}_R = (E_x, H_y) = (1,1)$ for a right-moving wave and $\vec{e}_L = (-1,1)$ for a left-moving one. Throughout this paper we restrict ourselves to materials without linear birefringence (in contrast with [29]). The O(2) symmetry about the axial direction implies, for the transport $\vec{v}_{i+1} = \mathcal{M}_i \vec{v}_i$, that the 4×4 $\mathcal{M}$ can be written (in this basis) in terms of the 2×2's M and C as $\mathcal{M} = \left(\begin{smallmatrix} M & C \\ -C & M \end{smallmatrix}\right)$, where C is only nonzero for transport that mixes the polarization states.

For dielectrics (also the only case we consider below), matrix M is proportional to the familiar 2×2 transfer matrix for individual polarizations. For example, for a unit intensity wave incident from the left, in steady state, the field amplitudes at the surface are $\vec{e}_{\text{in}} = (1,1) + r(-1,1)$, where r is the reflected amplitude. The outgoing field amplitude to the right of the system is given via $\vec{e}_{\text{out}} = t(1,1) = M\vec{e}_{\text{in}}$, where t is the transmission amplitude. In this basis, for a purely dielectric material of thickness L, index n,

$$M = \begin{bmatrix} \cos\delta & \frac{i}{n}\sin\delta \\ in\sin\delta & \cos\delta \end{bmatrix}, \tag{1}$$

where $\delta = nk_0L$ and k_0 is the vacuum wave number. Note that $\det(M) = 1$ always, but M_{11} and M_{22} are only equal in systems that have overall spatial parity symmetry. We identify the real part of the index n with refraction and its positive or negative imaginary part with absorption or gain.

Analytically for a slab dielectric Faraday rotator the M and C parts of the $\mathcal{M}$ in our field basis are [1,30]

$$M = \frac{1}{2}\begin{bmatrix} C_1 + C_2 & i(S_1/n_1 + S_2/n_2) \\ i(n_1S_1 + n_2S_2) & C_1 + C_2 \end{bmatrix} \tag{2}$$

and

$$C = \frac{1}{2}\begin{bmatrix} i(C_1 - C_2) & -(S_1/n_1 - S_2/n_2) \\ -(n_1S_1 - n_2S_2) & i(C_1 - C_2) \end{bmatrix}, \tag{3}$$

where $C_{1,2}$ ($S_{1,2}$) refer to the cosine (sine) of $\delta_{1,2} = n_{1,2}k_0L$ in which the n_1 and n_2 are the indices of refraction of the left- and right-circular polarization in the slab, k_0 refers to the vacuum wave vector, and L is the thickness of the slab. For a dielectric slab in an external magnetic field pointing along the direction of propagation, $\Delta n = n_1 - n_2 \propto VB$, the product of the Verdet and the magnetic field. Note that the resulting 4×4 matrix $\mathcal{M}$ is quite different from the one representing optical activity (a time-even rotation process), which has the form $M = \cos\alpha M_0$ and $C = \sin\alpha M_0$, where α is proportional to the density of chiral centers in the slab and M_0 is the usual 2×2 transfer matrix given by Eq. (1). Because CPR is a reversible optical process we require constant local power flux throughout in steady state. This condition thus requires the n's and the α to be real throughout for both the time-even and the time-odd rotation processes we consider below.

For a single polarization whose linear transport is given entirely in terms of a net 2×2 transfer matrix M in the basis described above and used throughout, the CPA state is reached when the condition $(1,1)M(1,1)^t = M_{11} + M_{12} + M_{21} + M_{22} = 0$ is satisfied. For a general 2×2 matrix, this condition combined with the determinant indicates that CPA implies four real conditions for four complex numbers. The remaining freedom of the optical field (amplitude and phase) then implies that CPA requires, at a minimum, tuning two dimensionless experimental parameters, typically, the ratio L/λ and the absorptive index $\text{Im}(n)$.

It is also straightforward to find the condition associated with CPR resonances using the 4×4 basis. For fields incident from the left, take $\vec{v}_l = (1,1,-l,l)$, where l is the amplitude of the reflected, rotated wave. On the right, take $\vec{v}_r = (-d,d,s,s)$; this configuration thus consists of incoming fields of one polarization and outgoing fields of the orthogonal polarization only, the CPR state. In analogy with the CPA state, these boundary conditions lead to a condition on the size, wavelength, and rotary power of the system. For CPR resonance in uniaxial systems with the 4×4 form of $\mathcal{M}$ as described earlier, we require

$$M\begin{pmatrix} 1 \\ 1 \end{pmatrix} + C\begin{pmatrix} -1 \\ 1 \end{pmatrix} l = \begin{pmatrix} -1 \\ 1 \end{pmatrix} d \tag{4}$$

and

$$-C\begin{pmatrix} 1 \\ 1 \end{pmatrix} + M\begin{pmatrix} -1 \\ 1 \end{pmatrix} l = \begin{pmatrix} 1 \\ 1 \end{pmatrix} s. \tag{5}$$

Counting the conditions (four complex) for the three complex fields (d,l,s), we see that to achieve CPR by simultaneously solving Eqs. (4) and (5) requires, at a minimum, tuning two experimental parameters (here, generically, the ratio L/λ and the circular birefringence $\Delta n = n_1 - n_2$), which we note is analogous to the CPA case (where the parameters are (L/λ) and the absorption coefficient). Eliminating the fields d, l, s, we can write the CPR condition succinctly for a general $\mathcal{M}$ as a single complex condition $\det(R) = 0$, where the 2×2

matrix R has the following elements:

$$R_{11} = (-1,1)C^{-1}M\begin{pmatrix}-1\\1\end{pmatrix}, \tag{6}$$

$$R_{12} = -(-1,1)C^{-1}\begin{pmatrix}1\\1\end{pmatrix}, \tag{7}$$

$$R_{21} = (1,1)[MC^{-1}M + C]\begin{pmatrix}-1\\1\end{pmatrix}, \tag{8}$$

$$R_{22} = -(1,1)MC^{-1}\begin{pmatrix}1\\1\end{pmatrix}. \tag{9}$$

We now summarize CPR phenomenology in a series of optical systems in order to build a deeper intuition about the CPR state and its connection to and contrast with CPA, with an eye towards its potential utility in optical devices.

III. CPR IN MODEL SYSTEMS

A. CPR in layered binary systems

Studying CPR in multilayer interference films provides a straightforward comparison of CPR and CPA phenomena and their dependence on dispersion, both material and structural. For simplicity, consider, first, a perfectly periodic multilayer composed of N alternating layers of a material A that is a dielectric with a zero Verdet and a material B that has a nonzero Verdet. We compare these systems to the CPA model system in which the bilayers have one nonabsorbing species (A) and the other absorbing (B). In all the model systems described here, only the B species rotates (for CPR) or absorbs (for CPA). The species have different indices of refraction in the absence of a magnetic field (for CPR) or absorption (for CPA), which we denote n_A and n_B, creating an optical (reflection) band gap. We denote these layered systems $(AB)^N$, but here, to eliminate any spurious effect from explicitly broken parity, we restrict our attention to parity-symmetric layered systems formed by adding one terminal A layer, that is, $(AB)^N A$.

One finding of these simulations (see Fig. 2) is that for the lowest thresholds, layered films with an odd number of bilayers (e.g., 31 layers) had threshold CPR states of even parity, and those with an even number of bilayers (e.g., 33 layers) had threshold CPR states of odd parity. A simple explanation for this observation is given in the next subsection (Sec. III B), on the consequences of parity symmetry (and parity breaking).

Note also that the wavelength at which the lowest CPR resonance occurs is at a band edge. As is well known, across the reflection band gap there is pronounced optical dispersion, resulting in large increases in the group velocity delay symmetrically at the band edges and significant reductions in the delay in the middle of the band. (Reference [32] is a recent relevant summary.) The reduction in the threshold for CPR or CPA with increases in the group velocity delay at the band edge is most clearly seen by plotting the product of the threshold value of the rotary power of the B layers times the number of layers versus the number of layers, as in Fig. 3 [dashed (green) trace], which hews closely to a plot of the group velocity minima versus the number of layers [solid (red) trace].

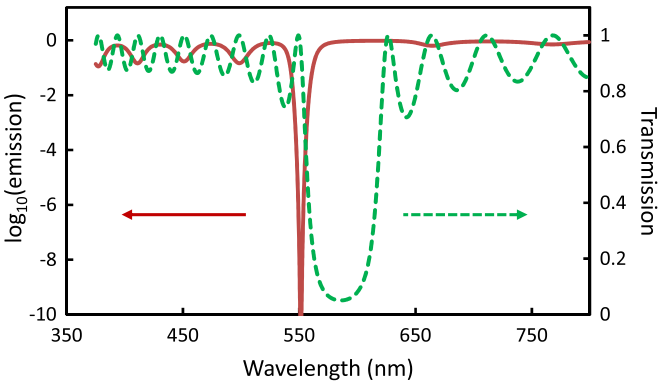

FIG. 2. (Color online) Typical CPR resonance in a one-dimensional photonic crystal. The dashed (green) trace is the transmission trace and the solid (red) trace is the total output light in the same polarization as the input polarization. This example is 31 alternating layers (each 100 nm thick) of index 1.55 (non-Faraday) and 1.38 (Faraday), corresponding to the first row in Table I [31]. Clearly shown in the dashed (green) trace is the reflection band gap that extends from 550 to 625 nm. The CPR resonance is the pronounced reduction in the output light polarized along the input polarization for wavelengths near the short-wavelength edge of the band.

Changes in the group velocity delay are, in and of themselves, not enough to explain the pattern of CPR (and CPA) resonances in these systems; the lowest threshold for the CPR or CPA resonances for $n_A > n_B$ occurs on the short-wavelength side of the band gap, but for $n_A < n_B$ it occurs at the long-wavelength edge of the band gap. As the time reverse of CPA, actual lasing [33], indicates, the simplest way to explain this difference is by apportioning the group velocity delay across the two species of the multilayer and noting that only in the B species is the light subject to polarization rotation (CPR) or absorption or gain (CPA

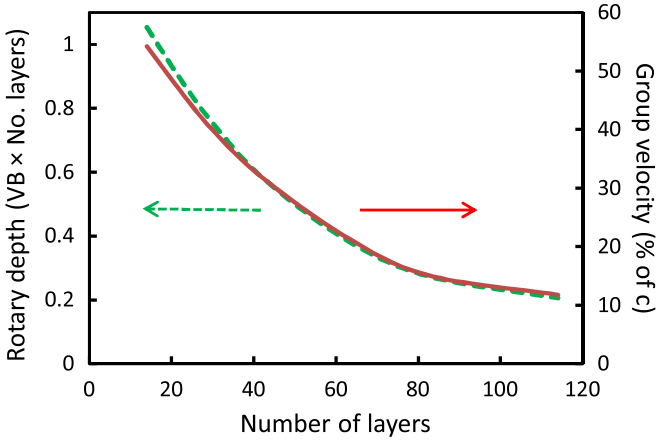

FIG. 3. (Color online) Correspondence between the group velocity delay and the CPR thresholds in layered media [left axis; dashed (green) trace]. Varying the number of layers only, we plot the CPR threshold Verdet-magnetic field product (VB) times the number of layers versus the number of layers. We also plot the group velocity minimum at the band edge versus the number of layers [right axis; solid (red) trace].

or lasing). Simulations of the local electric field of the light traversing the multilayer indicate that, off-band, the apportionment of the total velocity delay should follow the ratio of the indices. Near the long-wavelength side of the band edge, however, the light's integrated electric energy is higher in the larger index species, whereas the reverse occurs at the short-wavelength edge of the band gap [34]. Equating the field energy to the probability that the light will visit that species, and apportioning part of the total propagation time (and thus the overall Faraday rotation) to each species in proportion to that probability, qualitatively explains both the wavelength and the threshold of the CPR or CPA resonances.

Just as in CPA, there are other CPR states that arise at different wavelengths as Δn is increased beyond threshold. Note that for these simple binary multilayers, the next-to-lowest CPR resonance typically occurs at the opposite band edge, as expected and formerly noted [12] for CPA. To summarize the results from this study of CPR in multilayers in experimental terms, a 0.76-mm-thick multilayer of 160-nm layers of each bismuth-substituted iron garnet (BIG; index of refraction of $\sim$2.3 at 633 nm, at which the Verdet is $\sim -7 \times 10^3$ rad/Tm [30]) and ordinary SiO_2 glass would achieve CPR at 0.5 T, whereas a slab of BIG of length 2.4 cm would be needed at this field, indicating in concrete terms the substantial reductions in CPR thresholds associated with photonic bands.

In practice, with real multilayer systems, nonideality typically moves the lowest CPR or CPA threshold states from the band edge to defect states in the band gap itself. This is consonant with the experience in lasing, where it is well documented that layer nonuniformity and other perturbations cause lasing to occur first through defect states typically located within the band gap itself. The defect states still correspond to maxima of the group velocity delay [35]. (See the discussion of parity breaking in Sec. III B.)

It is illustrative to compare thresholds for CPA (lasing) and CPR in simple multilayer systems with deliberate structural defects, such as "phase-slip" (sometimes called "folded") distributed-feedback systems [34,36]. Here we compare the multilayers $(AB)^N(BA)^N$ and $(BA)^N(AB)^N$, where the time-odd process (either Faraday rotation, in the case of CPR, or absorption or gain, in the case of CPA/lasing) again occurs only in the B layers. Table II lists calculated threshold Δn values for CPR for four configurations of simply folded symmetric systems, which agree qualitatively with the corresponding results for CPA or lasing summarized in Fig. 4 (adapted from Ref. [37]). For example, controlling for overall gain, the folded distributed-feedback structure with the lowest lasing threshold (as inferred from the largest gain in the figure) is that which has the gain medium in the low-index material and is folded on the low-index layer. This result agrees with our simulations of the CPR threshold as reported in Table II (folded on B, $n_A > n_B$).

For contrast, we conclude this section with a case in which dispersion, but not field placement, is important: the loaded optical cavity as a layered optical system. Consider a dielectric Faraday rotator inside an optical cavity composed of transversely isotropic perfectly thin mirrors of reflectivity amplitude r (so that the reflectivity is $R = |r|^2$). The mirrors are represented by the transfer matrix $\mathcal{M}_r = \left[\begin{smallmatrix} M_r & 0 \\ 0 & M_r \end{smallmatrix}\right]$, where

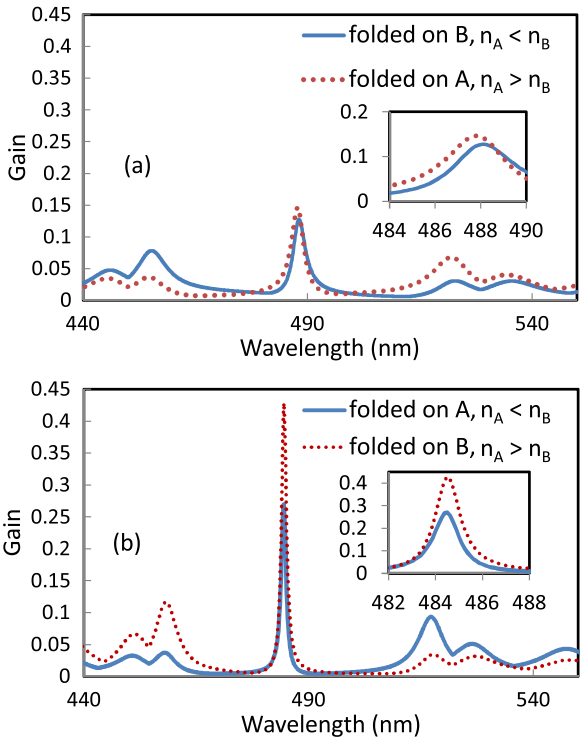

FIG. 4. (Color online) Transmission gain versus wavelength for folded structures analogous to those in Table II, where, instead of rotation in the B layers, a complex index of refraction is used to represent the optical gain. In this case the optical band stretches from 450 to 520 nm, and the prominent fold defect state appears near the center of the band. (Figure adapted from Ref. [37] with permission of The Optical Society of America.)

the 2×2 matrices M_r for the simple case of completely nonabsorbing mirrors are given in our "field" basis as $M_r = \frac{1}{\sqrt{1-|r|^2}}\left[\begin{smallmatrix} 1 & i|r| \\ -i|r| & 1 \end{smallmatrix}\right]$. Algebra indicates that all effects of the cavity reflectivity modify the conditions for CPR via a single parameter, $\gamma = \frac{2|r|}{1+|r|^2}$. One finds for this loaded cavity configuration (mirror-rotator-mirror) that the CPR condition becomes (compare the $r \to 0$ limit with Eq. (14) in Ref. [1])

$$\left(n_1 + \frac{1}{n_1}\right) S_1 C_2 - \left(n_2 + \frac{1}{n_2}\right) S_2 C_1 + \gamma \left(\frac{n_1}{n_2} - \frac{n_2}{n_1}\right) S_1 S_2 = \pm \left[\left(n_1 - \frac{1}{n_1}\right) S_1 - \left(n_2 - \frac{1}{n_2}\right) S_2 + 2\gamma (C_2 - C_1)\right], \quad (10)$$

where, as before, $n_{1,2} = n_0 \pm \Delta n/2$ and $k_0 \Delta n = 2VB$.

To compare this result with CPA, it is straightforward to show that the lowest CPA resonance threshold for a cavity loaded with a lossy dielectric modeled as a complex index n is given by the solution of [compare with the $r \to 0$ limit of Eq. (7) in Ref. [2], also reproduced in Eq. (13) here for completeness]:

$$e^{i2nk_0L} = \frac{(n-1)^2 - (n^2+1)\frac{2R}{1+R} + i\gamma(n^2-1)}{(n+1)^2 - (n^2+1)\frac{2R}{1+R} + i\gamma(n^2-1)}. \quad (11)$$

In Fig. 5, we have used Eq. (11) for $n_0 = 2.0$ and $k_0 L \sim 820$ to plot the fractional reduction in the lowest CPR resonance threshold (Δn) as a function of the reflectivity, R. The graph

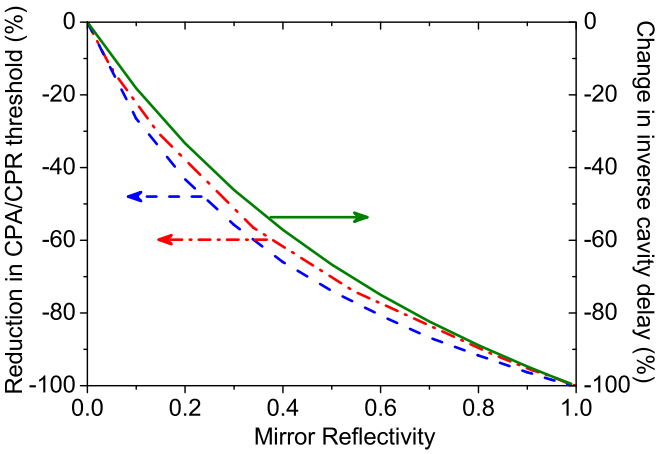

FIG. 5. (Color online) The lowest CPR [dot-dashed (red) trace] and CPA [dashed (blue) trace] resonance thresholds in a loaded cavity decrease as one increases the finesse of the mirrors, going to 0 with the inverse of the group velocity delay [solid (green) trace].

shows a strong similarity to the inverse of the time spent in the cavity (i.e., the fractional reduction in the group velocity), as expected, and also corresponds with the reduction in the CPA threshold of an absorber-loaded cavity shown in the graph. Not shown in Fig. 5, we have also analyzed a realistic (e.g., complex dielectric) gold mirrored cavity at 780 nm and found qualitatively the same behavior as in Fig. 5 with increasing gold layer thickness. In that study there are no 780-nm CPA states from tuning the loss in the dielectric slab inside the cavity if the gold layer thickness exceeds 35 nm (corresponding to an R of about 85% in each mirror) because at that depth the absorption in the gold itself is above the CPA threshold.

B. CPR with explicitly broken parity

In a parity-symmetric absorbing structure, the fields of all CPA states must also be of definite parity, even or odd. These two possibilities generally occur at different absorption thresholds. Since we have already discussed layered optical systems, one particularly intuitive way to understand this difference is shown in Fig. 6, where one of the species (B) is absorbing (or rotating, in the CPR case) and the other species (A) is

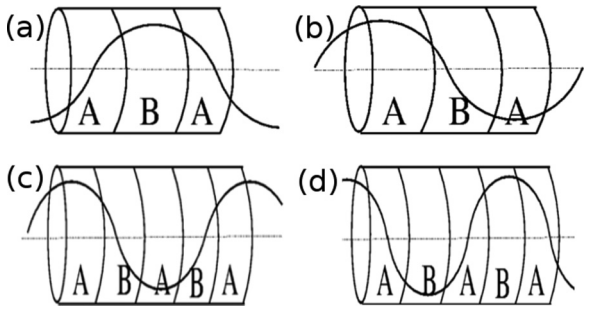

FIG. 6. Parity and CPA or CPR. For an odd number of bilayers, we see that (a) the even-parity fields have a maximum on the B species, whereas (b) in the odd-parity case, the field on the B layer is significantly smaller. For an even number of bilayers, however, the situation is reversed, so that (c) even-parity fields do not have their maxima on the B layers, but (d) odd-parity fields do.

TABLE I. CPR thresholds (Δn values for the circular polarization propagation eigenstates in layer B) at the reflection band edge for the layered binary systems described in Fig. 2. Here and in Table II the letters after the threshold values indicate the spatial symmetry (O, odd; E, even) of that CPR resonance's fields.

Configuration	31 layers	33 layers
$n_A > n_B$	0.049(E)	0.044(O)
$n_A < n_B$	0.090(E)	0.080(O)

not. For wavelengths nearly four times the layer thickness (near the band edge), as in the example shown in Fig. 6, the even-parity case has a larger field overlap on the absorber or rotator (species B) than the odd-parity field for an odd number of bilayers (in this case, one bilayer), thus the former will have a lower CPA threshold (compare with Table I).

When a rotator (absorber) is not parity symmetric, there are still CPR (CPA) states, but the state's fields will not be of definite parity. To illustrate the effect of parity breaking on CPR and its comparison with CPA (see Refs. [5,38]), in this section we consider two examples of parity-broken systems: (i) an $(AB)^N A$ multilayer, but with layer-to-layer thickness variations, and (ii) a trinary regular layered system of type $(ABC)^N$ [in both cases only B is rotary (CPR) or absorptive (CPA)].

As one introduces layer thickness variations into the $(AB)^N A$ structures discussed in Sec. III A, formerly localized reflection band states mix with extended states, whereas some formerly extended states become localized [35]. Initially, weak localization increases the group velocity delay and thus reduces the CPA or CPR threshold for some states near the band edge (see Fig. 7 for one example). As the localization length shrinks further with increasing layer thickness variations, random scattering reduces the coherent band edge reflections that were responsible for the increase in the group velocity delay in the first place. As the level of randomness is increased, the lowest resonant CPR or CPA state's wavelength at threshold moves into what was previously the reflection band. Note also that adding layer thickness randomness explicitly breaks the original parity symmetry of the system. As a consequence, at finite randomness in the CPA case, the amplitude ratio of the input fields is no longer ± 1.

The consequence of parity breaking through broken structural symmetry in CPR is different from that in CPA [39]. Solving Eqs. (4) and (5) for the amplitude ratio of the incident

TABLE II. CPR threshold values of Δn for "folded" layered systems comprised of 52 total layers. Every entry is for a CPR resonance occurring on the defect state inside the reflection band. The lowest CPR threshold occurs with even parity when rotation occurs in the lower index material and the fold is on that low-index material. CPR threshold ordering in the chart is in one-to-one agreement with that of lasing thresholds in these "folded" distributed-feedback systems reproduced in Fig. 4.

Configuration	Fold on A	Fold on B
$n_A > n_B$	0.032(O)	0.013(E)
$n_A < n_B$	0.017(E)	0.028(O)

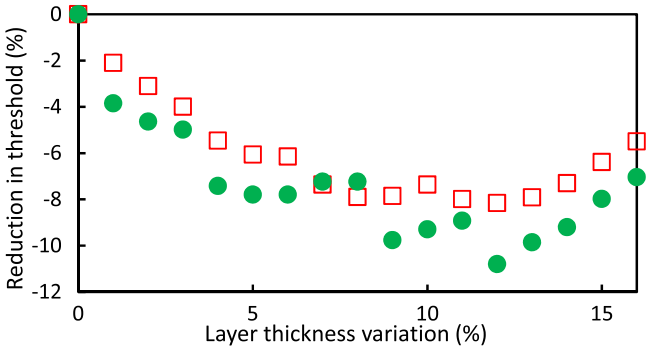

FIG. 7. (Color online) Percentage reduction of CPR [filled (green) circles] and CPA [open (red) squares] in the thresholds for the lowest CPR or CPA state, which, as described in the text, occur near the band edge. For this example, a particular random layer thickness variation map for the 65-layer multilayer with $n_B > n_A$ [only species B is Faraday (CPR case) or absorptive (CPA case)] is programmed into the simulation and increased across the horizontal axis.

fields, l, indicates that

$$l = \frac{(M_{11} + M_{12} + M_{21} + M_{22})}{(C_{11} + C_{21} - C_{12} - C_{22})} = \frac{(C_{11} + C_{21} + C_{12} + C_{22})}{(M_{22} + M_{12} - M_{11} - M_{21})} \tag{12}$$

in the CPR state. For any optical system composed of sections without birefringence or optical activity, it was shown in Ref. [1] that the 4×4 $\mathcal{M}$ has underlying 2×2 matrices M and C, with the M being time-even and of the form $\left[\begin{smallmatrix} \mathcal{R} & \mathcal{I} \\ \mathcal{I} & \mathcal{R} \end{smallmatrix}\right]$ and the C being time-odd and of the form $\left[\begin{smallmatrix} \mathcal{I} & \mathcal{R} \\ \mathcal{R} & \mathcal{I} \end{smallmatrix}\right]$, where $\mathcal{R}$ means a purely real quantity and $\mathcal{I}$ a purely imaginary one. This matrix structure in the formulas for l gives $|l| = 1$, which in turn forces all the optical fields to have the same intensity for a CPR state in any system. The broken parity in the CPR state is instead manifest by the appearance of mismatched phases (not shown) between the input fields.

Explicit parity breaking via structural asymmetry is also evident in the trinary films, $(ABC)^N$, again, in which only B is rotary (CPR) or absorptive (CPA). As an example, Table III reports a comparison of the CPR and CPA lowest resonance thresholds near the band edges of the very first reflection band of trinary films. Thus, even for perfectly ordered trinary films, it is the phase mismatch between the left and the right input fields that varies universally, while the amplitude ratios only vary for the CPA case. Note also that the threshold values for the cases $n_A > n_C > n_B$ and $n_B > n_A > n_C$ are ordered the same in both CPR and CPA. In particular, for each of these cases in Table III, the CPR or CPA state forms at the appropriate band edge as discussed in the previous section. The spectral location of the CPR or CPA state in the intermediate case $n_A > n_B > n_C$ depends on the indices' values.

TABLE III. Thresholds for $(ABC)^N$ layered systems where the indices of refraction are chosen from the list $\{1.55, 1.51, 1.38\}$ and the total number of layers is 45 (each layer is 100 nm thick).

Type	Configuration	Threshold	Amplitude ratio
CPR	$n_A > n_C > n_B$	0.0465	1
CPR	$n_A > n_B > n_C$	0.0652	1
CPR	$n_B > n_A > n_C$	0.0752	1
CPA	$n_A > n_C > n_B$	0.0528	1.44
CPA	$n_A > n_B > n_C$	0.092	0.215
CPA	$n_B > n_A > n_C$	0.087	1.52

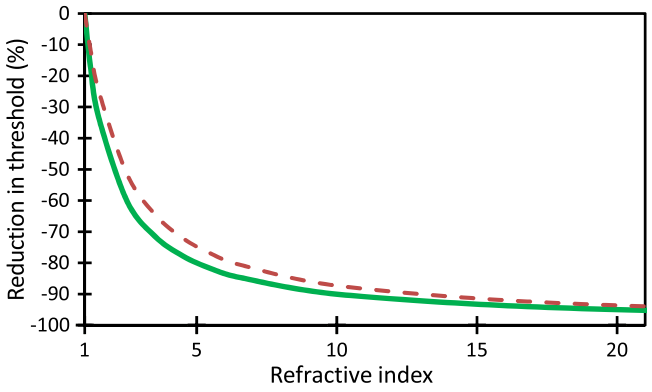

FIG. 8. (Color online) CPR threshold reduction [dashed (red) trace] is monotonic to 0 as the index of refraction of the slab is increased, following the same relation as in the CPA case [$\sim 1/n$ at large n as described in the text; here, the solid (green) trace].

Two additional facts of interest emerge from these simulations. As one might expect, the intensity ratios are more varied for the trinary films (explicit parity breaking) than for the random $(AB)^N A$ layered system (which breaks parity more softly) studied here to only 15% layer thickness variation. Also, for the case of random $(AB)^N A$ layered systems, the variation in the phase is much larger in the CPR case than in the CPA case. Note in this regard that the CPR state forces the intensity ratio to remain unity, whereas for CPA both the amplitude ratio and the phase adjust to remain resonant in a parity-broken system.

C. Combined Faraday rotation and optical activity

To highlight the time-reversal symmetries underlying CPR and CPA, we now address the effect that the time-even part of the transport has on the CPR or CPA threshold. In the original derivation of the CPR effect [1] in a simple slab dielectric, increasing the index of refraction of the material reduces the CPR threshold, as shown graphically in Fig. 8 using the formula in Ref. [1]. This is also the case with the CPA threshold, which (see Eq. (7) in Ref. [2]), for an absorbing slab dielectric of index $n = n_0 + i n_{\rm abs}$ and length L, is

$$e^{ink_0 L} = \pm \frac{(n-1)}{(n+1)}. \tag{13}$$

In the large-n_0 limit, because the log is vanishing as $\sim 1/n_0^2$, the threshold $n_{\rm abs}$ must decrease as $\sim 1/n_0$ at large n_0. A graph of this reduction of CPA in a bulk absorber from Eq. (13) is included in Fig. 9(b). We note in passing that this reduction is what one would expect for the single-transit-time reduction, and not that associated with the etaloning as was the case for the optical-cavity-assisted reduction in the thresholds.

In CPA, the index of refraction real and imaginary parts can be considered the time-even and time-odd contributions

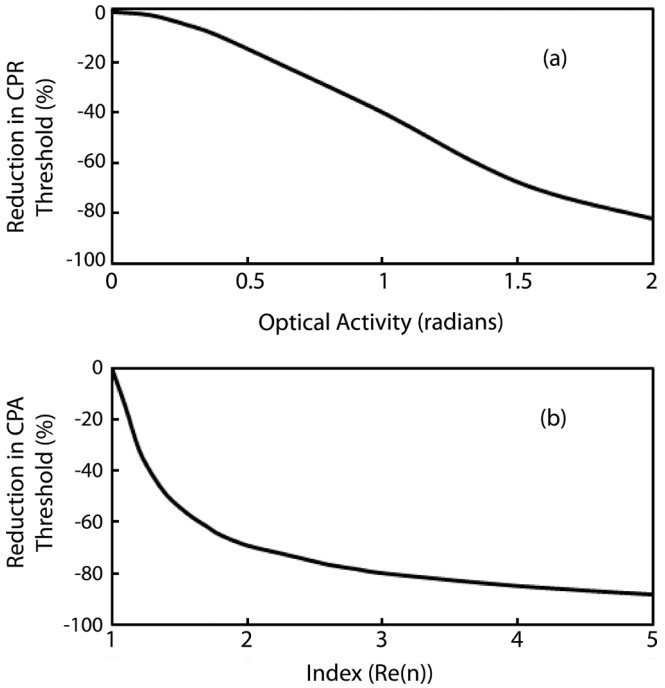

FIG. 9. The lowest CPR and CPA resonance thresholds decrease monotonically to 0 as the time-even part of the transport is increased. (a) Reduction in CPR threshold for a Faraday (time-odd) constituent sandwiched between two optically active slabs as a function of the total optical activity of the time-even part alone (in radians). (b) Reduction in CPA threshold as a function of the real part of the material's refractive index.

to the transport. The analogous processes for transport of the polarization are optical activity (time-even) and Faraday rotation (time-odd). Recall that one cannot achieve CPR with optical activity alone, but the question we would like to address is how the presence of optical activity in a system modifies the threshold Faraday rotation needed for CPR.

Consider a system with both of these processes operating. Instead of a single bulk piece, for simplicity we analyze a three-layer system composed of two optically active blocks with a Faraday rotator in between. [See discussion following Eq. (1) for the matrix representation of optical activity.] It is then straightforward to identify the CPR state in this system, again in terms of the equation $\det(R) = 0$, where the matrix elements of the 2×2 complex matrix R are as in Eqs. (6)–(9), but where we make the substitutions for M and C via

$$\begin{pmatrix} M \\ C \end{pmatrix} = \begin{pmatrix} \cos 2\alpha & -\sin 2\alpha \\ \sin 2\alpha & \cos 2\alpha \end{pmatrix} \begin{pmatrix} M_0 M M_0 \\ M_0 C M_0 \end{pmatrix}, \qquad (14)$$

where M_0 is given by Eq. (1) for the optically active blocks (with chiral density proportional to α) and the M and C on the right-hand side of Eq. (14) are given by Eqs. (2) and (3), respectively, for the Faraday block. Keeping the indices and length the same, and changing only the optical activity, we can determine the location of the CPR state [see Fig. 9(a)]. We see that, as in the decrease in the CPA threshold with increasing real part of the refractive index n_0, the Faraday rotation needed to achieve CPR resonance decreases monotonically as the optical rotation in the adjoining slabs is increased. We note that this reduction continues with increasing optical activity beyond the value at which the optical rotary part of the assembly by itself would rotate a single input ray to its orthogonal polarization (rotation by $\pi/2$) upon exiting in transmission. This result is true for both positive and negative Verdet values, irrespective of the handedness of the optical activity; the trace in Fig. 9(a) is symmetric about zero optical activity. Both of these (CPR and CPA) curves asymptote to zero threshold.

This shows that increasing the time-even part of an optical process reduces the time-odd threshold for achieving CPR or CPA and is expected to be useful for reducing the size, complexity, and cost of devices based on CPR or CPA, for example, by reducing the required magnetic field.

IV. CONCLUSIONS

CPR and CPA are phenomenologically congruent in how their thresholds depend on the system's symmetry, composition, and geometry. As both are coherent perfect processes, this congruence follows from the underlying commonality they share through wave interference and time reversal symmetry. Furthermore, this study reveals potential design routes to decrease the size and/or magnetic field requirements for achieving CPR. For example, as detailed above, multilayering the rotating species can yield a 30-fold reduction in the naive length-field product. Similarly, even a poor optical cavity with just 60% reflective mirrors reduces the CPR threshold length-field product by nearly 80%. By layering with suitable optically active materials, high-index materials, tertiary layered systems, and layered systems with small layer thickness variations in the stack, we have shown that further reduction in the naive length-field product is achievable in CPR-based devices.

ACKNOWLEDGMENTS

The authors are grateful to the National Science Foundation for financial support under Grant No. ECCS-1360725 and to the National Science Foundation for financial support from the Science and Technology Center for Layered Polymeric Systems under Grant No. DMR 0423914.

[1] M. Crescimanno, N. J. Dawson, and J. H. Andrews, Phys. Rev. A **86**, 031807(R) (2012).

[2] Y. D. Chong, L. Ge, H. Cao, and A. D. Stone, Phys. Rev. Lett. **105**, 053901 (2010).

[3] W. Wan, Y. Chong, L. Ge, H. Noh, A. D. Stone, and H. Cao, Science **331**, 889 (2011).
[4] S. Longhi, Phys. Rev. A **82**, 031801(R) (2010).
[5] Y. D. Chong, L. Ge, and A. D. Stone, Phys. Rev. Lett. **106**, 093902 (2011).
[6] S. Longhi, Phys. Rev. Lett. **107**, 033901 (2011).
[7] Z. Lin, H. Ramezani, T. Eichelkraut, T. Kottos, H. Cao, and D. N. Christodoulides, Phys. Rev. Lett. **106**, 213901 (2011).
[8] A. Mostafazadeh, Phys. Rev. A **87**, 012103 (2013).
[9] S. Dutta-Gupta, O. J. F. Martin, S. Dutta Gupta, and G. S. Agarwal, Opt. Express **20**, 1330 (2012).
[10] S. Dutta-Gupta and G. S. Agarwal, Opt. Lett. **39**, 390 (2014).
[11] S. Longhi, Phys. Rev. A **83**, 055804 (2011).
[12] Y. Shen, L. Shen, Z. Lai, G. Wang, and X. Deng, Phys. Lett. A **378**, 299 (2014).
[13] C. Y. Huang, R. Zhang, J. L. Han, J. Zheng, and J. Q. Xu, Phys. Rev. A **89**, 023842 (2014).
[14] Y. Nakata, Y. Urade, T. Nakanishi, and M. Kitano, Phys. Rev. B **88**, 205138 (2013).
[15] M. Kang, F. Liu, T.-F. Li, Q.-H. Guo, J. Li, and J. Chen, Opt. Lett. **38**, 3086 (2013).
[16] X. Luo and L. Yan, IEEE Photon. J. **4**, 590 (2012).
[17] Z.-R. Zhang, H.-Q. Li, H. Chen, C.-L. Hu, and P. Zhou, Eur. Phys. Lett. **105**, 47008 (2014).
[18] S. Feng and K. Halterman, Phys. Rev. B **86**, 165103 (2012).
[19] K. Egashira, A. Terasaki, and T. Kondow, Eur. Phys. J. D **66**, 92 (2012).
[20] Y. D. Chong and A. D. Stone, Phys. Rev. Lett. **107**, 163901 (2011).
[21] L. Ge, Y. D. Chong, S. Rotter, H. E. Tureci, and A. D. Stone, Phys. Rev. A **84**, 023820 (2011).
[22] M. Pu, Q. Feng, M. Wang, C. Hu, C. Huang, X. Ma, Z. Zhao, C. Wang, and X. Luo, Opt. Express **20**, 2246 (2012).
[23] R. Bruck and O. L. Muskens, Opt. Express **21**, 27652 (2013).
[24] X. Fang, M. L. Tseng, J.-Y. Ou, K. F. MacDonald, D. P. Tsai, and N. I. Zheludev, Appl. Phys. Lett. **104**, 141102 (2014).
[25] R. R. Grote, J. B. Driscoll, and R. M. Osgood Jr., Opt. Lett. **38**, 3001 (2013).
[26] T. Chen, S. Duan, and Y. C. Chen, J. Opt. Soc. Am. A **29**, 689 (2012).
[27] S. Dutta-Gupta, R. Deshmukh, A. V. Gopal, O. J. F. Martin, and S. Dutta Gupta, Opt. Lett. **37**, 4452 (2012).
[28] G. Pirruccio, G. Lozano, Y. Zhang, S. R. K. Rodriguez, R. Gomes, Z. Hens, and J. G. Rivas, Phys. Rev. B **85**, 165455 (2012).
[29] Y. Wang, M. Pu, C. Hu, C. Hu, Z. Zhao, C. Wang, and X. Luo, Opt. Commun. **319**, 14 (2014).
[30] H. Kato, T. Matsushita, A. Takayama, M. Egawa, K. Nishimura, and M. Inoue, J. Appl. Phys. **93**, 3906 (2003).
[31] These somewhat arbitrary values were chosen for their utility in multilayer CPA/lasing modeling and to be consistent with previous studies by the authors [37], and they do not affect the conclusions drawn here.
[32] M. Crescimanno, G. Mao, J. Andrews, K. Singer, E. Baer, A. Hiltner, H. Song, K. Comeau, B. Shakya, A. Bishop, and R. Livingston, J. Opt. Soc. Am. B **29**, 1038 (2012).
[33] J. P. Dowling, M. Scalora, M. J. Bloemer, and C. M. Dowden, J. Appl. Phys. **75**, 1896 (1994).
[34] J. H. Andrews, M. Crescimanno, K. D. Singer, and E. Baer, J. Poly. Sci. B: Poly. Phys. **52**, 251 (2014).
[35] Y. Wu, K. D. Singer, R. G. Petschek, H. Song, E. Baer, and A. Hiltner, Opt. Express **17**, 18038 (2009).
[36] E. Yablonovitch, Phys. Rev. Lett. **58**, 2059 (1987).
[37] J. H. Andrews, M. Crescimanno, N. J. Dawson, G. Mao, J. B. Petrus, K. D. Singer, E. Baer, and H. Song, Opt. Express **20**, 15580 (2012).
[38] M. Kang, F. Liu, and J. Li, Phys. Rev. A **87**, 053824 (2013).
[39] In CPR, parity is not broken explicitly by the magnetic field (a pseudovector) itself.